

CHARACTERIZING THE PERFORMANCE OF THE SR-30 TURBOJET ENGINE

T. Witkowski, S. White, C. Ortiz Dueñas, P. Strykowski, T. Simon

University of Minnesota

Introduction

“What?!!” exclaimed one student. “Thermodynamics doesn’t work! Why am I even studying this stuff?!” She was taking her senior lab – an engine lab with the SR-30 engine – and the numbers didn’t work out... on purpose. The professor had set it up that way.

The SR-30 is a small-scale, turbojet engine which sounds and smells like a real engine used to fly commercial aircraft. With an overall length of less than 2.0 feet and an average diameter of 6.5 inches, the SR-30 is equipped with an inlet nozzle, radial compressor, counter-flow combustion chamber, turbine, and exhaust nozzle. Although it can operate on various fuels, diesel fuel is used in the studies described here, and each component is instrumented with thermocouples and pressure gages to allow a complete thermodynamic evaluation. Screaming along at 80,000 rpm and sending out exhaust gas at 500 mph, the SR-30 engine is fun science for students! However, since the SR-30 was essentially designed for one-dimensional measurement and flow analysis, students quickly learn the limitations of these assumptions.

SR-30 Thermodynamic Analysis

The SR-30 gas turbine is modeled by the Brayton cycle which employs air as the working fluid. The basic process is to compress the air, add fuel, burn the air-fuel mixture, and use the energy released to develop thrust. Since the SR-30 engine is not attached to a moving airplane, a bellmouth inlet nozzle is used to create a uniform velocity profile at the compressor inlet and minimize losses. The Brayton cycle for the SR-30 thrust turbine is composed of the following processes:

- 1) Isentropic acceleration through an inlet nozzle
- 2) Isentropic compression
- 3) Constant pressure heat addition through combustion chamber
- 4) Isentropic expansion through turbine
- 5) Isentropic expansion across an exhaust nozzle

Each process in the Brayton cycle can be analyzed individually using the laws of thermodynamics. A simple, one-dimensional analysis assumes steady-state, steady-flow conditions for the processes, uniform properties at each state location, and negligible changes in potential energy. Changes in kinetic energy are assumed to be negligible everywhere except across the exhaust nozzle, though they are recognized to be important within the compressor and turbine systems. By selecting appropriate control volumes (e.g. compressor, combustor, turbine, nozzle) and applying these assumptions, the equations of mass and energy conservation and an entropy balance produce,

$$\sum \dot{m}_{in} = \sum \dot{m}_{out}$$

$$\dot{Q} - \dot{W} = \sum \dot{m}_{out} \left[h_{out} + \frac{V_{out}^2}{2} \right] - \sum \dot{m}_{in} \left[h_{in} + \frac{V_{in}^2}{2} \right]$$

$$0 = \sum_j \frac{\dot{Q}_j}{T_b} + \sum \dot{m}_{in} \cdot s_{in} - \sum \dot{m}_{out} \cdot s_{out} + \dot{\sigma}$$

where the subscript j represents the discrete locations on the control volume where the heat transfer occurs; T_b is the temperature at that boundary, and sigma is internal irreversibility. Every component except the combustor is assumed to be adiabatic and hence $\dot{Q} = 0$. Likewise, if a process is adiabatic and reversible, it is isentropic such that the second law of thermodynamics yields $\Delta s = 0$. These equations are applied to each component of the SR-30 engine, and the efficiency of each component is defined as the ratio of the actual behavior to the ideal model. Figure 2 shows a cross-section of the SR-30 engine with the state numbers used in the analysis.

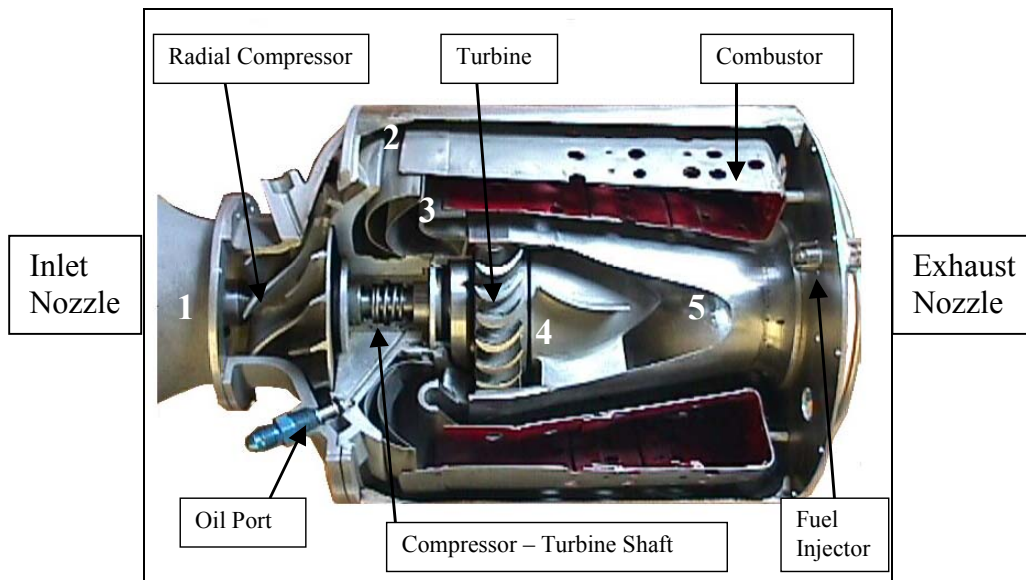


Figure 1. Cut-away View of the SR-30 Engine. State Locations: 1. Compressor Inlet; 2. Compressor Outlet; 3. Turbine Inlet; 4. Turbine Outlet; 5. Nozzle Exit.

Note that the radial compressor and the counter-flow combustion chamber maintain a compact engine size as well as allow a short compressor-turbine shaft an advantage when balancing the engine at speeds up to 100,000 rpm. In correspondence with the states labeled in Figure 1, the following analysis of the engine is performed, assuming ideal characteristics.

System Components

The inlet nozzle directs air into the compressor. The air flowing into the nozzle is assumed to take place isentropically and determines State 1 for the thermodynamic cycle. The SR-30 is instrumented with a Pitot-static tube in the inlet nozzle, which is used to measure the differential pressure of the flow entering the engine. The static pressure, P_1 , is then calculated assuming the total pressure, P_{1t} , is atmospheric pressure, which is monitored independently (the subscript ‘t’ refers to stagnation conditions). The mass flow rate of air is estimated by assuming a constant velocity and density profile over the inlet area. Properties are evaluated using the ideal gas law, and the intake velocity is estimated from the Pitot-static tube, assuming incompressible flow conditions.

The radial compressor takes the inlet air and compresses it from State 1 to State 2 to provide air to the combustion chamber. Because heat loss from the compressor is assumed to be small compared to the change in enthalpy of the air passing through the compressor, the compressor is modeled as adiabatic. The power required by an adiabatic compressor is determined by the expression:

$$\dot{W}_c = \dot{m}_a (h_{t1} - h_{t2}),$$

where the traditional thermodynamic sign convention has been adopted. In the combustor fuel mixes with the compressed air and burns. The chemical energy of the fuel is converted to molecular kinetic energy, raising the temperature of the products of combustion and the excess air. The sophistication with which the combustion analysis is performed depends on the level of the student conducting the SR-30 laboratory. For purposes here, the combustor has been modeled as a steady-state device having energy streams as indicated in Figure 2.

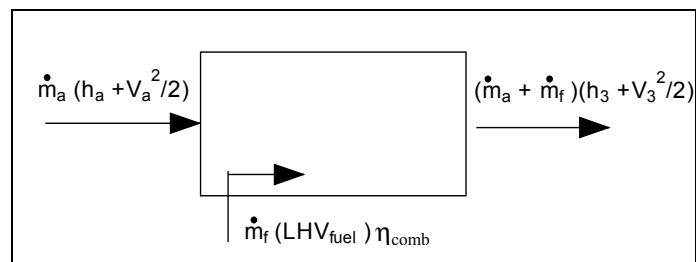


Figure 2. Simplified Thermodynamic Model of the Combustion Process

The turbine extracts the molecular kinetic energy, i.e. internal energy, from the products of combustion and converts it to shaft work. In developing power, the gas loses internal energy and cools down. Similar to the compressor, the turbine power developed is determined by the expression:

$$\dot{W}_T = (\dot{m}_a + \dot{m}_f) \cdot (h_{t3} - h_{t4})$$

After leaving the turbine, the engine exhaust is directed through an isentropic, exit nozzle to the atmosphere. The SR-30 engine contains a subsonic exhaust nozzle, meaning that the pressure at the nozzle exit (P_5) is equal to the ambient pressure. There are no shocks within the nozzle. The same approach used with the inlet nozzle is taken at the exhaust nozzle such that the exhaust velocity (V_5) is estimated, i.e. uniform flow conditions are initially assumed.

After passing through the turbine, the gases still contain large amounts of internal energy. If these gases are allowed to expand and accelerate, they will convert the energy contained in the molecular kinetic energy of the molecules into bulk kinetic energy of the flow, thereby providing thrust. Engine thrust is the difference of the products of the intake mass flow and velocity and the exit mass flow and velocity, which when assuming no pressure thrust takes the form:

$$T_x = (\dot{m}_a + \dot{m}_f) \cdot V_5 - \dot{m}_a \cdot V_{aircraft}$$

In the laboratory, the SR-30 engine is mounted on a test stand, so that far upstream of the engine we can take $V_{aircraft} = 0$.

The analysis discussed is ideal, and measurements taken by students will typically yield erroneous results based on these assumptions. As the discussion to follow will attest, students will quickly learn the limitations of one-dimensional thermodynamic analysis for the treatment of a real jet engine. Measurement probes in the SR-30 engine are designed to accommodate their repositioning as desired. This feature allows the instructor to place these probes in locations that will lead to apparent violations of the first and second laws of thermodynamics. Integral analysis can then be executed to illustrate proper closure of the equations and calm students' nerves about the thermodynamic foundations they have come to view as sacred.

SR-30 Data Collection and Results

During engine start up, there is a period of time where temperature variations are observed. These thermal transients are dependent on the initial starting conditions of the engine, and after time, tend to reach steady-state, steady-flow conditions. All conditions discussed below are provided for a fixed engine speed of 70,000 rpm ($\pm 2\%$).

Three start-up conditions were tested. The cold start was a normal start, after the engine had been idle for a period of over 24 hours. All engine components were at room temperature ($\sim 18^\circ\text{C}$). The medium and hot starts were actually restarts, after the engine had been operating. The engine was shut down with standard operating procedures. Using an external compressed air supply to spin the compressor-turbine spool, the engine was then cooled by drawing in room temperature air; component temperatures were monitored during this period. The engine was restarted when

safe starting conditions were achieved. Table 1 describes the starting conditions for the three cases examined at 70,000 rpm.

Start Type	T _{t2}	T _{t3}	T _{t4}
Cold	18°C	18°C	18°C
Medium	40°C	40°C	50°C
Hot	60°C	80°C	100°C

Table 1. Engine Restart Conditions

As seen in Figure 3, the compressor temperature (T_{t2}) reaches nominally steady-state conditions after approximately 20 minutes of operation. Temperature measurements at the other locations, shown in Figure 4, do not converge as consistently as those at the compressor. For the measurements of the combustor (T_{t3}), turbine exit (T_{t4}) and nozzle exit (T_{t5}), the temperatures vary, and tend to converge differentially between 10-20 minutes, with some variations still noticeable after 25 minutes. The data suggest that a start-up period on the order of at least 10 minutes is required to achieve quasi-steady state conditions. This can be very nicely accommodated by first demonstrating the engine to the students prior to data acquisition.

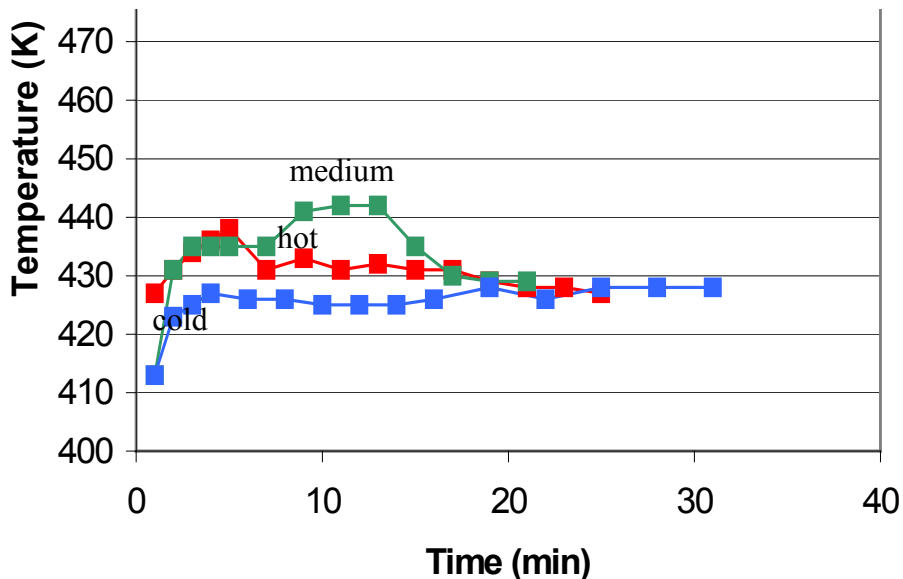


Figure 3. Compressor Exit Temperature (T_{t2}) for Three Start-up Conditions at 70,000 rpm

During data collection, temperature and pressure measurements at the nozzle exit are taken by two different sets of probes mounted in the nozzle exit plane at the rear of the engine. One set of temperature and pressure probes (State 5) is used to take point measurements at the seven o'clock position, looking upstream, of the exhaust nozzle exit plane. Another set of probes is mounted on a traverse at the exit plane of the nozzle to obtain detailed profile measurements. The traversing probe location is referred to as State 6; detailed exhaust flow analysis is performed using the exhaust profile temperatures and dynamic pressures.

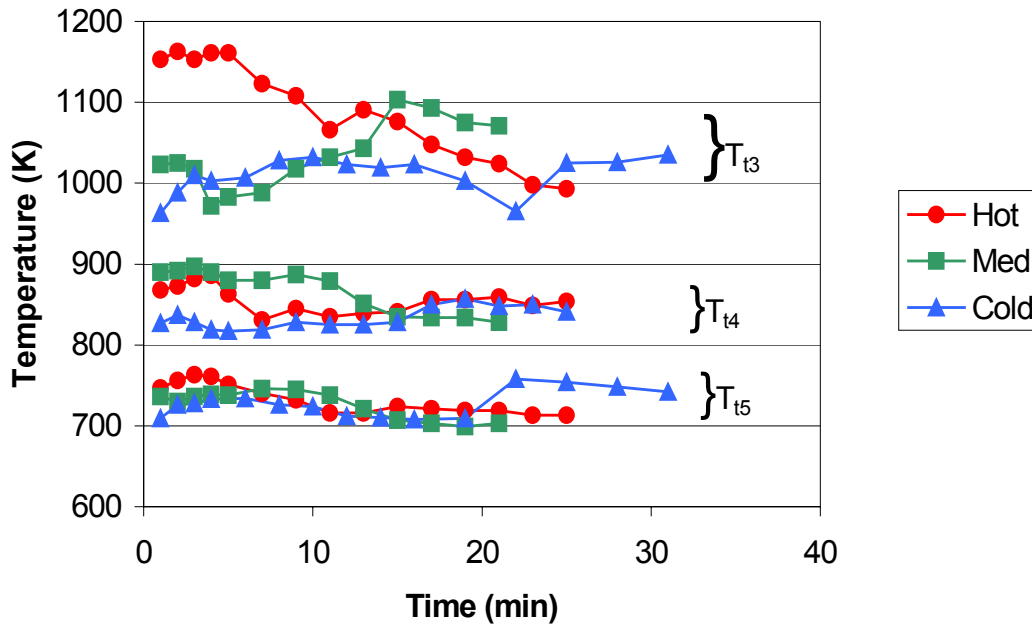


Figure 4. Temperature Measurements within the SR-30 Engine for Various Start-up Conditions at 70,000 rpm.

Thermodynamic analysis of the SR-30 engine is very sensitive to the location of the sensors, in particular the placement of thermocouples at State 2 (compressor outlet) and State 3 (turbine inlet). What follows is an example of data that can be used to illustrate this concept to students. The data sheet provided as Table 2 is used to assist students in acquiring the basic engine thermodynamic states. The table allows the student to monitor States 1-5 over a 10 minute development period, which typically is conducted after an initial 10-15 minute warm-up period. While engine transients are relatively small, the exercise of documenting the states over time is a useful reminder of the concept behind the steady-state assumption.

T ambient	19	C				
p ambient	29.99	in. Hg				
Engine RPM	70000	+/-		1000		
	2 min	4 min	6 min	8 min	10 min	Average
T1 (°C)	20	20	20	20	20	20
T2 (°C)	184	187	189	189	188	187.4
T3 (°C)	727	735	720	748	734	732.8
T4 (°C)	615	608	603	621	616	612.6
T5 (°C)	use T6	use T6	use T6	use T6	use T6	use T6
p1 (torr)	16.21	16.73	16.66	16.56	16.5	16.532
p2 (psig)	17	17	17	17	17	17
p3 (psig)	17	18	18	18	18	17.8
p4 (psig)	1.5	1.4	1.4	1.4	1.3	1.4
p5 (psig)	use p6	use p6	use p6	use p6	use p6	use p6
pfuel (psig)	68	67	68	68	67	67.6

Table 2: Data Sheet Used to Acquire Thermodynamic State Information

“Proceedings of the 2003 American Society for Engineering Education Annual Conference & Exposition Copyright © 2003, American Society for Engineering Education”

In addition to the single-point data collected in Table 2, students conduct a 30-point traverse of total pressure and temperature across the nozzle exit plane (State 6). The nozzle exhaust data are carefully integrated to evaluate exit mass flow, kinetic energy, and thrust. Independent measurements are also made to accurately determine fuel flow rates from the fuel pressure indicated in the table. Entries for temperature and pressure at State 5 are not recorded since the detailed profile is captured at the nozzle exit; T_5 , however, is monitored continuously by the engine operator to avoid excessive exhaust gas temperatures.

In the example data set provided in Table 2, the thermocouple probe at State 2 was intentionally positioned too close to the inner wall of the passageway between the engine outer housing and the combustion chamber. Employing the thermodynamic analysis outlined earlier, the data from Table 2 results in an input compressor power of 34.9 kW and a turbine output power of 28.3 kW. Since the compressor must drive the turbine as well as overcome bearing friction, the experimental finding that the turbine power is less than the compressor power leaves most students flabbergasted. “Impossible!” some say. “Wow, this is an efficient engine!” say others. “These gages must be broken!” says another. There is no lack of opinions on what is transpiring.

The objective here is to teach students to troubleshoot rather than to give up. Interactive lab discussions can be devised to provoke further thought. The instructor can formulate this scenario into a “real life, on the job” situation: What would the student do if this happened at work and her boss was depending on her to have results by the end of next week for an important presentation to upper management? Instructor creativity here is key and will motivate students to dig deeper.

In reality, the temperature within the engine at State 2 varies significantly across the section, and placement of the thermocouple near the inner wall results in a T_2 measurement significantly higher than the bulk average needed for thermodynamic closure. How would the students have known this a priori? Limitations of the one-dimensional analysis are illustrated by the poor and unrealistic results obtained. Ultimately, an integrated temperature value taken over the radial distance from the inner wall to the outer wall of the compressor is needed in order to supply a practical answer. The instructor will direct the students to look closer at the exhaust nozzle profile for clues. The temperature profile leaving the nozzle is “ugly” and anything but uniform. If such distinct radial temperature variations can be seen across the exhaust nozzle, perhaps similar non-uniformities exist elsewhere in the engine. At this point students have spent 4-5 hours in the lab and are finished for the day. They will resume this discussion when they return for their second 5-hour session the following week.

The depth to which thermocouple T_{12} (State 2) can be inserted into the engine is determined by the radial distance between the compressor walls. The outer wall of the compression chamber is the outer casing of the engine, while the inner wall of the compression chamber is the outer wall of the combustor. The outside diameter of the engine is 171 millimeters. At the location of the T_{12} thermocouple, the compressor chamber is 10 mm wide.

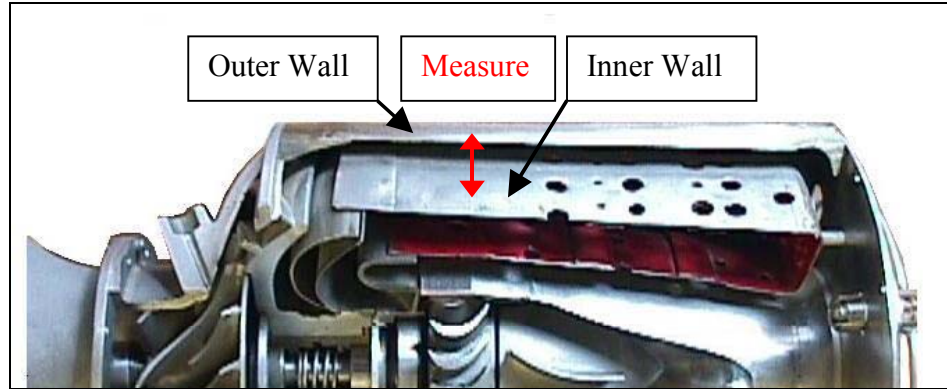


Figure 5. Compressor Chamber

Temperature measurements were taken at locations across this chamber, starting at the outer wall and going to the inner wall. There is a significant temperature gradient across this chamber as seen in Figure 6. There is approximately a 50-70°C temperature difference from the inner wall to outer wall at all engine speeds investigated. However, the pressure across the compression chamber did not vary by a measurable amount.

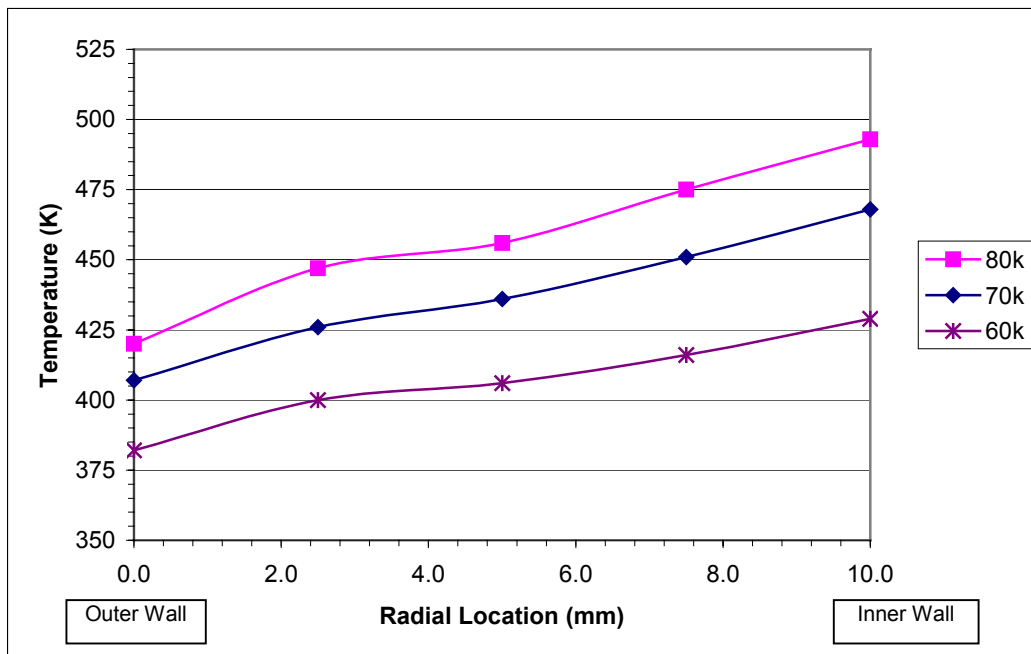


Figure 6. Temperature Profile Across Compressor Chamber

The compressor temperature measurements at State 2 determine the enthalpy of the compressed air. If a uniform velocity profile is assumed, the total enthalpy of the flow can be integrated across the compressor chamber, using the measured temperature profile. Another method is to take the average temperature measured across the profile and use that value to determine the enthalpy of the flow. A third method is to use the midpoint temperature to calculate enthalpy. Table 3 shows that the results of these three methods differ only slightly.

Engine Speed	Wc Integrated	Temperature Average	Wc Average	Temperature Midpoint	Wc Midpoint
RPM	kJ/s	K	kJ/s	K	kJ/s
60,000	-20.1	406.9	-20.1	406	-20.1
70,000	-36.1	437.6	-36.1	436	-35.9
80,000	-49.8	458.6	-50.0	456	-49.4

Table 3. Compressor Work Calculated Three Ways

In the same manner that incremental measurements were taken across the compressor outlet, traverse measurements can be taken across the combustion chamber. It is important to note, however, that no profile measurements have been recorded at the exit of the turbine due to the difficulty of traversing a probe at State 4.

The instrumentation error in the previous example represented by Table 2 was corrected by placing thermocouple T_{12} at the midpoint between the compressor walls. Data was then collected during normal operation of the SR-30 engine at 70,000 rpm. The results of this analysis are shown in Table 4.

Engine Thrust	44 N
Thermal Efficiency	3.65 %
Compressor Work	28.27 kW
Turbine Work	28.33 kW
Compressor Efficiency	54.44 %
Turbine Efficiency	72.85 %
Combustor Efficiency	98.34 %
Air-Fuel Ratio	68.58 ---
Inlet Air Flow Rate	0.206 kg/s
Fuel Flow Rate	0.003 kg/s
Exhaust Gas Flow Rate	0.209 kg/s
Pattern Factor	0.704 ---

Table 4. SR-30 Analysis Results

Teaching with the SR-30 Engine

Classroom learning often provides students with the initial data required to solve a problem, thus focusing the students' attention on theoretical principles, scientific laws, and how physical phenomenon can be modeled using scientific equations. Laboratory learning, however, presents a great opportunity to expose young minds to the practical methods used to obtain input data as well as realistic results. For example with the SR-30 engine, students are exposed to some of these methods when attempting to calculate the fuel flow rate, the bulk velocity in and out of nozzles, and integrated values.

Fuel Flow Rate

The fuel flow rate in cc/min is given by the equation

$$\text{fuel flow rate} = 4.07P_{\text{manifold}} - .013P_{\text{manifold}}^2 - 3.7$$

where P_{manifold} is the fuel manifold pressure measured in psig from the gage on the test stand. This equation was obtained by weighing the fuel tank prior to and after test runs of 30 minutes and curve fitting the data. Errors in the fuel flow are attributed entirely to the precision error in P_{manifold} . Although it is not feasible to have students derive this flow rate equation during an engine analysis lab, a separate lab to determine the fuel flow rate is possible. The objective is to (1) allow students to experience taking several measurements to obtain one value – the fuel flow rate, and (2) to perform several unit conversions as the professor mentions that in practical experiments, input data is not often given in the desired units, i.e. gage readings must be converted to *absolute* values to analyze data, etc.

Inlet Nozzle Velocity

These calculations expose students to how Pitot-static tube measurements are used to calculate nozzle velocity. The pitot-static tube used at State 1 in the SR-30 laboratory at the University of Minnesota has one hole located on the tube nose and additional holes located on the tube sides. The nose of the tube is placed parallel to the velocity stream, and the Pitot-static tube gage measures the differential pressure across the holes. Pressure at the nose is treated as P_t since flow 'stops' at the nose, while pressure at the sides is the actual pressure at that location since flow at the sides is at the mainstream velocity. The inlet nozzle velocity is measured as follows.

- The pressure gage at State 1 measures a differential pressure, P .
- $P = P_t - P_1$
- $P_t = \text{atmospheric pressure}$
- Students solve for P_1 and use this value in their analysis.

Integration

Without the use of a data acquisition system, it is necessary to integrate profile data by hand in order to achieve realistic results. At State 6 (the exhaust nozzle exit), temperature and pressure

probes are mounted on a traverse which is moved across the exit plane of the nozzle using a micrometer. The nozzle is 54 millimeters in diameter. The upper most location of the probes is set when the micrometer traverse reads -3 mm. Measurements are taken at regular intervals, and the probes are moved until the micrometer reads +51mm. Students are required to find the differential area associated with each data point as well as the local velocity and the local density. These numbers are used to find the exhaust flow rate at that point. Ultimately, to complete the integration, the flow rates at each point are summed to determine the exhaust gas flow rate for the profile. This calculation forces students to see a practical application for the integration they learned in calculus class, thereby enhancing their learning experience.

Although these calculations may seem simple and be subconscious operations to a learned experimentalist, the professor must remember that labs are often a college student's first experience with applying the theoretical principles she has learned in class. Combining several of these techniques in one lab is more than enough complexity to stimulate creative and analytical thinking in a student.

Recommendations

A complete thermodynamic analysis along with several teaching techniques and practical methods to obtain realistic results have been described throughout this paper. The SR-30 engine provides many more fun opportunities to puzzle as well as dazzle students while exploring the world of jet engines. Substances may be placed in the exhaust stream to make visible the escaping gas. For example, copper strips placed in the velocity field downstream of the exhaust nozzle would turn this high temperature gas green. Professors may choose to give point data rather than profile data at the exhaust nozzle exit (rather than the compressor exit) to baffle students. Data acquisition systems can be added to the engine to measure real time temperatures and pressures. This provides the opportunity of adding a load cell to the engine stand to measure thrust and have students compare that value with their integrated values. Many parameters can be altered or added in order to teach students to think when conducting laboratory experiments. The lesson learned with the student who believed that thermodynamics did not work – it is not usually the scientific principle that is wrong, but the operator or the experimental setup! Professors should strive to make learning a joy. The next John Barber, Nicholas Otto, or Robert Goddard may be sitting in one of their classrooms.

Appendix: Turbomachinery Analysis of the SR-30 Gas Turbine Engine

The discussion to follow summarizes a more advanced analysis of the radial compressor and axial turbine of the SR-30 engine. Notation changes slightly to accommodate traditional nomenclature in turbomachinery analysis; subscript ‘o’ refers to stagnation conditions, c to absolute velocity, w to blade relative velocities, and U to blade speed.

In order to better understand the performance of the SR-30 gas turbine engine a one-dimensional turbomachinery analysis was done using the Engineering Equation Solver (EES) software. The objective of this analysis was to independently compute the flow through the radial compressor and through the one-stage axial turbine using only the size dimensions of each component and the initial conditions of the flow entering each component (given by reliable experimental measurements). The challenge was to accurately identify the sources of losses and to accurately predict and estimate them. Once the losses were estimated the efficiencies for each component were calculated. This analysis was done at a rotational speed of $N = 78,000$. An Engineering Equation Solver (EES) program was developed to compute velocities and thermodynamic states of the flow at different points within the compressor and the turbine.

One-dimensional Analysis

The locations of points at which velocities and thermodynamic states were computed, shown in Figure 1A, are:

- 1 Entrance to impeller
- 2 Exit of Impeller-entrance to vaneless diffuser
- 2' Exit of vaneless diffuser – entrance to vaned diffuser
- 3 Exit of vaned diffuser
- 4 Entrance to turbine stator
- 5 Exit from turbine stator – entrance to turbine rotor
- 6 Exit from turbine rotor

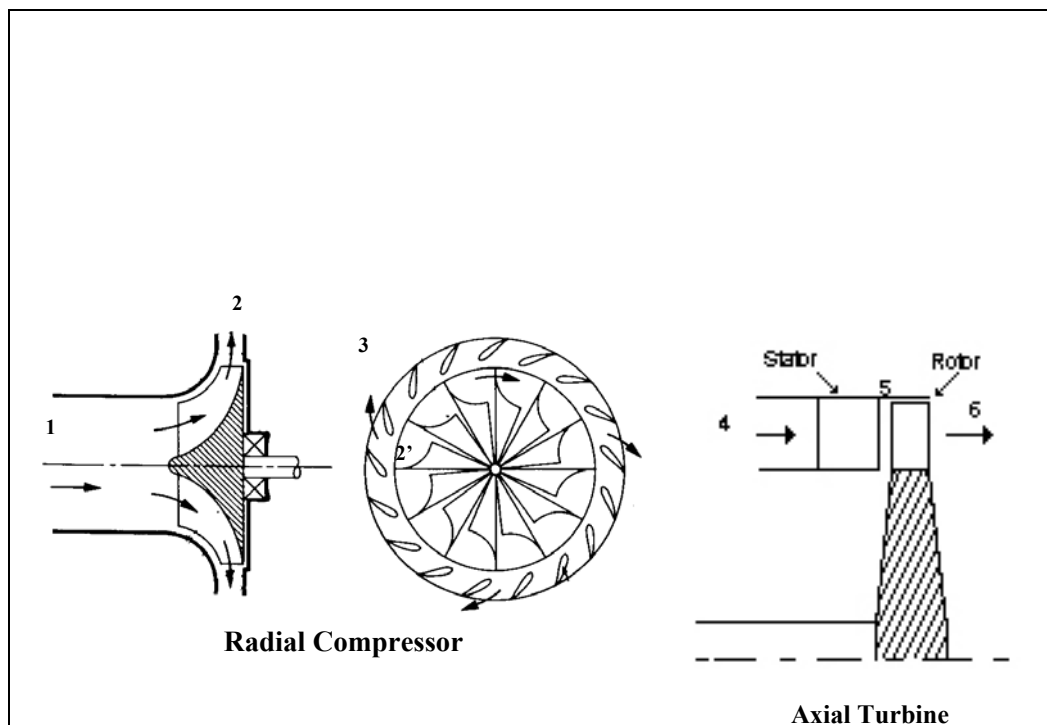


Figure 1A. Location of points at which velocities and thermodynamic states were calculated.

The following equations were used throughout the analysis for both the compressor and the turbine:

Mass Flow Rate

$$\dot{m}_{compressor} = \rho_1 c_1 A_1 \quad \dot{m}_{turbine} = \rho_4 c_4 A_4$$

Stagnation and Static Conditions were calculated using the following formulas:

$H_0 = c_p \left(T + \frac{c^2}{2} \right)$, $P_0 = P(s_0, H_0)$, and $T_0 = T(s_0, H_0)$ where s_0 is the entropy at stagnation conditions.

No work in the diffuser of the compressor or the nozzle of the turbine:

$$T_{02} = T_{03} \quad \text{and} \quad T_{04} = T_{05}$$

Euler's turbomachinery equation:

$$h_{02} - h_{01} = U_2 c_{\theta 2} - U_1 c_{\theta 1} \quad \text{and} \quad h_{06} - h_{05} = U(c_{\theta 6} - c_{\theta 5})$$

Radial Flow Compressor

The objective of this analysis is to compute the flow through the radial flow compressor of the SR-30 gas turbine engine. Actual images of the compressor turbomachinery are shown in Figure 2A.



Figure 2A. From left to right: top view of impeller, side view of impeller, vaneless and vaned diffusers.

The dimensions of the compressor and the initial conditions of the flow entering the impeller are given in Table 1A. Performance characteristics such as stagnation pressure ratio, compressor shaft work, and compressor total-to-total efficiency are computed. The results at each location are given in Table 2A.

Table 1A Dimensions of the radial compressor and inlet conditions of the flow entering the impeller

Impeller	Diffusers	Inlet Conditions
$D_h=20.6\text{mm}$	$\delta = 4.76 \text{ mm}$ Radial width of vaneless diffuser	$P_{01} = 100 \text{ kPa}$ $T_{01} = 300 \text{ K}$ $c_{\theta 1}=0$ (no pre-swirl of the flow entering the impeller)
$D_s=60.3\text{mm}$	$b_2 = 55.76 \text{ mm}$ Radius at entrance of vaned diffuser	
$D_2=102\text{mm}$	$b_3= 78 \text{ mm}$ Radius at exit of vaned diffuser	
$\beta_1=-57 \text{ deg}$ and $\beta_2=-20 \text{ deg}$	$L = 60 \text{ mm}$ Diffuser vane length	
$b_2 = 6.35\text{mm}$, axial width at exit of impeller	$2\theta = 10.5 \text{ deg}$ Diffusion angle	
$c = 0.5 \text{ mm}$, Tip clearance, distance between rotor and stationary shroud		
$n_b=9$ primary blades and 9 secondary blades		

Table 2A Results of thermal and hydraulic analysis

	Inlet to Impeller	Exit of Impeller	Entrance to Vaned Diffuser	Exit to Vaned Diffuser
Subscripts	1	2	2'	3
Area	0.002522 m ²	0.001714	0.001874	0.002622
P ₀	100 kPa	323 kPa	319 kPa	269 kPa
T ₀	300 K	445 K	445 K	445 K
P	93.6 kPa	167 kPa	199.5 kPa	269 kPa
T	294 K	379 K	390 K	430 K
Abs. velocity c and M_{abs}	106 m/s 0.31	366.5 m/s 0.87	335.2 m/s 0.86	175.6 m/s 0.42
Rel velocity w and M_{rel}	195 m/s * 0.57 / max 0.84	123 m/s 0.31		
U	163.7 m/s	416.6 m/s		
Entropy s	5.702 kJ/kgK	5.764 kJ/kgK		5.782 kJ/kgK
* opposite to rotation				

Velocity Diagrams

The velocity diagrams for the impeller are shown in Figure 4A. The slip is calculated using Stodola's equation, where n_b is the number of blades at the exit of the impeller:

$$|\Delta w_{\theta}| = |\Delta c_{\theta}| = \frac{\pi U_2}{n_b} \cos \beta_2'$$

The actual slip in the analysis was taken to be 40% of that computed from Stodola's model, the choice of the value was somewhat arbitrary, but a substantially lower value was needed because the exit channel of the impeller is very narrow and Stodola's model does not account for this low aspect ratio.

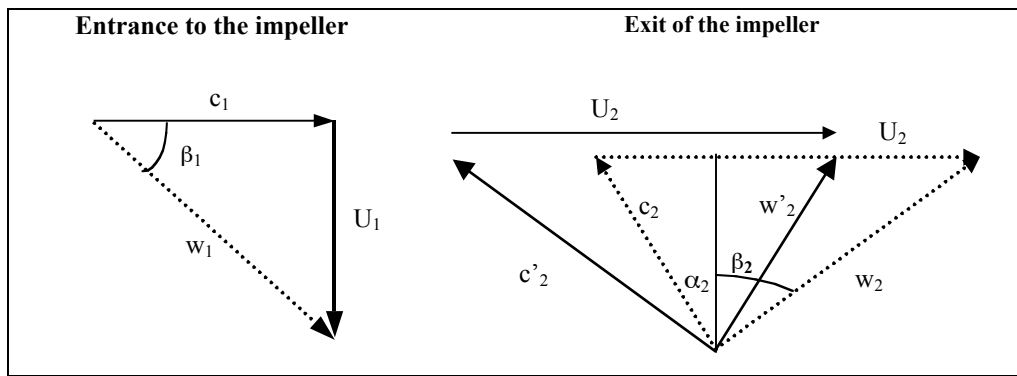


Figure 3A. Impeller velocity diagrams

The velocity diagram for the diffuser is shown in Figure 5A. Within the vaneless diffuser, the following conditions were used:

Free vortex: $c_{\theta 2} r_2 = c_{\theta 2'} r_2'$
 Mass conservation: $\rho_2 c_{r 2} r_2 = \rho_2 c_{r 2'} r_2'$

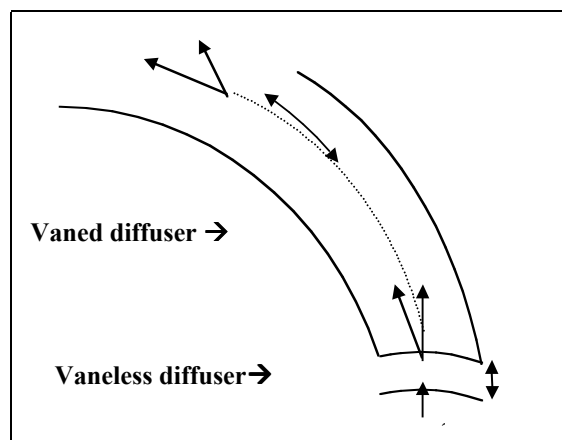


Figure 4A. Diffuser velocity diagram

Losses

In the analysis of real performance, losses must be accounted. The SR-30 engine is considerably smaller than a conventional engine. The small scale tends to lead to larger losses due to larger leakage path sizes as a fraction of engine size.

The rotor tip speed and ambient conditions are about the same for this engine as for larger engines e.g. auxiliary power unit (APU) or an aircraft engine. Thus, the absolute and relative velocities, as well as the velocity diagrams will be comparable to those of an aircraft engine. The key parameter to consider is the Reynolds number. This dimensionless number is a measure of the inertial forces versus viscous forces, and it varies linearly with the length scale and rotor speed. For this engine, the Reynolds number of the rotor inlet relative flow, defined as follows, is:

$$Re = \rho_1 w_1 H / \mu = 214580 \sim 2.4 \times 10^5$$

$$H = r_{\text{shroud}} - r_{\text{hub}} - \text{tip clearance}$$

where the subscript 1 defines conditions at inlet of the compressor and H is the rotor blade chord. The Reynolds number for an aircraft engine is of the order 10^6 , an order of magnitude larger than that of our engine. This means that the viscous effects are expected to be more important in the SR-30 engine, which, in turn, will affect the loss calculations. Jacobson¹ computed scaling relationships for a micro turbine (an order of magnitude smaller than our engine), which will be used here as approximations to provide a feel for the effects of the scale for our compressor analysis.

The different equations and scaling factors used to estimate the loss coefficients for the impeller are shown in Table 3A. The first column in this table shows the different types of losses that were predicted to be present in the flow through the impeller. The second column shows the values of loss coefficients for each of these losses obtained from the literature for a normal size aircraft engine. The third column shows the Jacobson's scaling factor, Sf, which takes into account the Reynolds number previously mentioned. Jacobson estimated different scaling factors for each type of loss. The fourth column shows the scaled loss coefficients.

Table 3A. Estimation of impeller losses

IMPELLER			
$\Delta P_{o \text{ loss}} = \lambda (P_{o1r} - P_1)$			
Parameter (Approximate length the flow travels in the impeller = 5 cm $b_2 = 0.00535 \text{ m}$)	Calculated losses for the SR-30 engine, λ	Jacobson's¹ Scale Factor Sf $x = H = 0.02 \text{ m}, C = 18.5 \text{Re}^{-0.3}$	Scaled losses $\lambda_{sf} = \lambda * Sf$
Mean friction coefficient $f = 0.02$ $\lambda = fL/b_2$	0.18	$C/(x^{0.5}), Sf = 3.5$	$0.02 * 3.5 = 0.65$
Boundary layer displacement thickness/ passage width	0.09 (Using laminar flat plate bl sol. approx)	$2C/(x^{0.5}), Sf = 7.0$	$0.09 * 7.0 = 0.63$
Shear drag between rotating and stationary components	$\Delta \eta_c / \eta_c = -0.3 t / b_2$ $t \sim 0.0012 \text{ m}$	$0.039/x = 2.3$	$\Delta \eta_c / \eta_c = -0.3 * 2.3 t / b_2$ $\Delta \eta_c / \eta_c = -0.69 t / b_2$
Incidence Losses	0.2 (approx.)	No scaling	0.2
Recirculation Losses	$0.1 * (1/2 \rho_1 w_2^2) = 0.2$	No scaling	0.2
2-Dimensional Losses to 3-Dimensional Losses	$\Delta P_{o \text{ loss } 2D}$	Jacobson argues that 3-D modeling of micro turbines are a factor of 2 higher than those predicted by 2-D modeling	$\Delta P_{o \text{ loss } 3D} = 2 * \Delta P_{o \text{ loss } 2D}$

The diffuser can be a significant contributor of losses to the overall compressor efficiency. The diffuser section consists of two types of diffuser; a vaneless diffuser and a vaned diffuser (see Figure 2A). For this analysis, we assume that the vaneless diffuser has only an incidence loss in stagnation pressure of 3% of the inlet velocity head. The vaned diffuser for the SR-30 engine is

¹ Jacobson, S.A., *Aerothermal Challenges in the Design of a Microfabricated Turbine Engine*, MIT, AIAA-98-2545

not a straight or planar diffuser; it has vanes with high turning angles: cambered vanes (see Figure 2A). A cambered vaned diffuser has the advantage that it does not occupy much space and the disadvantage is that its efficiency is substantially less than for a planar diffuser. The vaned diffuser losses are summarized in Table 4A.

Table 4A. Estimation of vaned diffuser losses

Vaned Diffuser			
Parameter	Efficiency for planar diffuser	Efficiency for cambered diffuser	
Efficiency	80 %	50%	Reduction due to high turning angles, smaller scale approximation and 3-D flow
Blockage	-	0.15	approximation
Static Pressure recovery factor $C_p = (P_3 - P_2)/(P_{02} - P_2)$	-	0.58	From Kenny ² , DP, Diffuser effectiveness

Shock losses are not included in this analysis though they might play an important role. The inlet Mach number to the vaned section is 0.86. Although, not computed to be supersonic, this high Mach number could indicate that the flow would become sonic if any change occurred in the inlet conditions or in rotational speed.

Results

The results of the compressor analysis are summarized in Table 5A. The computed work is in line with measurements though the efficiency is higher than measured.

Table 5A. Summary of results

Mass flow rate	$m_{\dot{}}$	0.297 kg/s	Compressor Total to Total Efficiency	$\eta_c = (T_{03ss} - T_{01}) / (T_{03} - T_{01})$	72 %
M_{max} at inlet of impeller (tip)	w_{1max}/a_1	0.84	Impeller Efficiency	η_i	82 %
M_{max} at inlet of diffuser	c_2/a_2	0.86	Diffuser Efficiency	η_d	50 %
Impeller pressure ratio	p_2/p_1	1.94	Work	$W_{\dot{}} * m_{\dot{}}$	43.5 kW
Stator pressure ratio	p_3/p_2	1.48	Absolute Flow Angle at exit of impeller	α_2	73.5 deg
Static pressure change in the rotor	$(p_2 - p_1)/(p_3 - p_1)$	0.50	Reynolds number as defined previously	$\rho_1 w_1 H / \mu$	237047 ~ 2.4 x 10 ⁵
Stage stagnation pressure ratio	p_{03}/p_{01}	3.0			

² Kenny, D.P., *The History and Future of Centrifugal Compressor in Aviation Gas Turbines*, 1984. Values taken from reference in: Hill and Peterson, *Mechanics and Thermodynamics of Propulsion*, 1992.

Axial Flow Turbine

The objective of this analysis is to compute the flow through the axial flow turbine of the SR-30 gas turbine engine. Actual images of the turbine turbomachinery are shown in Figure 5A.

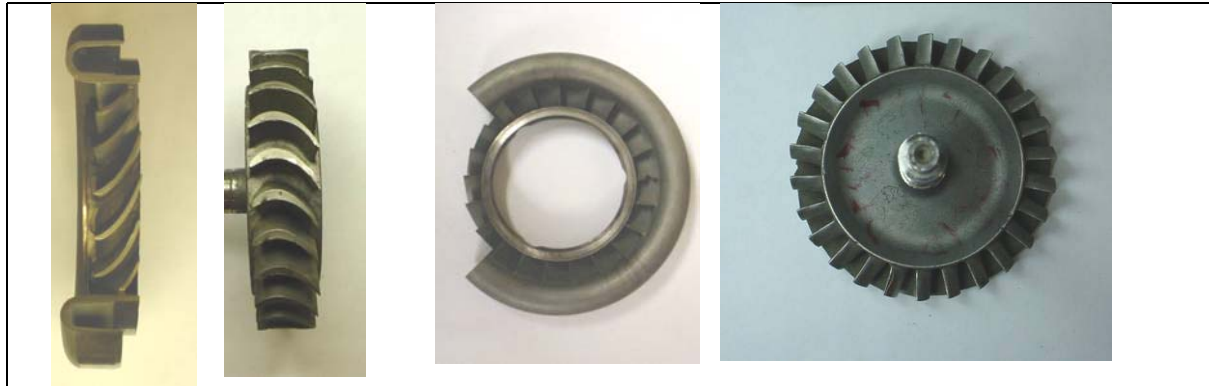


Figure 5A. From left to right: side view of the stator, side view of the rotor, top view of the stator, top view of the rotor.

The dimensions of the turbine stage and the initial conditions of the flow entering the stator are given in Table 6A. Performance characteristics such as total stagnation pressure ratio, turbine shaft work, and turbine stage total-to-total efficiency are computed.

Table 6A Dimensions of the turbine stage and inlet conditions of the flow entering the nozzle.

Rotor		Inlet Conditions
$D_h = 64 \text{ mm}$		$P_{01} = 250 \text{ kPa}$
$D_{tip} = 88.9 \text{ mm}$		$T_{01} = 973 \text{ K}$
$\beta'_2 = -58 \text{ deg}$ and $\beta'_3 = -68 \text{ deg}$	Blade angles with respect to the horizontal	$c_{\theta 1} = 0$ (no pre-swirl of the flow entering the impeller)
$t = 3 \text{ mm}$	Blade max. thickness	
$a = 10.3 \text{ mm}$	Point to max. thickness	
$L = 18.2 \text{ mm}$	Chord length	
$n_{b, \text{rotor}} = 26$	Number of blades in the rotor	
Stator: assume the blades have the same shape as the rotor blades		
$n_{b, \text{stator}} = 21$	Number of blades in the stator	

The locations of points at which velocities and thermodynamic states were computed are given in Fig 1A. The results at each location are given in Table 7A.

Table 7A Results of thermal and hydraulic analysis

	Inlet to Stator	Exit from Stator- and Entrance to Rotor	Exit from Rotor
Subscripts	4	5	6
Area	0.00299 m ²	0.00299 m ²	0.00299 m ²
P0	250 kPa	233.5 kPa	120 kPa
T0	973 K	973 K	841.3 K
P	93.6 kPa	127.6 kPa	115 kPa
T	294 K	833.5 K	832.4 K
Abs. velocity <i>c</i> and <i>M</i> _{abs}	114 m/s 0.19	556.8 m/s 0.98	140.8 m/s 0.25
Rel velocity <i>w</i> and <i>M</i> _{rel}		255 m/s* 0.45	260 m/s* 0.46
U		316.3 m/s	
Entropy <i>s</i>	6.673 kJ/kgK	6.692 kJ/kgK	6.721 kJ/kgK

* opposite to rotation

Velocity Diagrams

The velocity diagrams for the turbine stage are shown in Figure 4A. The incidence angle was found after an iteration process with different angles of incidence. It was found that the Mach number of the absolute velocity exiting the nozzle is very sensitive to this angle. The optimum angle was found to be $i = 5.5$ deg. This incidence angle gives the maximum work output without choking the nozzle.

The first approximation for the deviation was calculated using the following equation:

$$\beta_3 = -11.5 + 1.154 \cos^{-1} \Theta / s + 4s / e,^3$$

$$\delta = \beta'_3 - \beta_3$$

where $\Theta / s = 0.41$, Θ is the opening at the throat between two blades, s is the pitch of the blade, e is the mean radius of curvature and δ is the deviation. After substituting approximate values, we obtained: $\delta = 9$ deg. Following the same approach as for the calculation of slip in the compressor, the actual value used for the deviation was $1/3$.

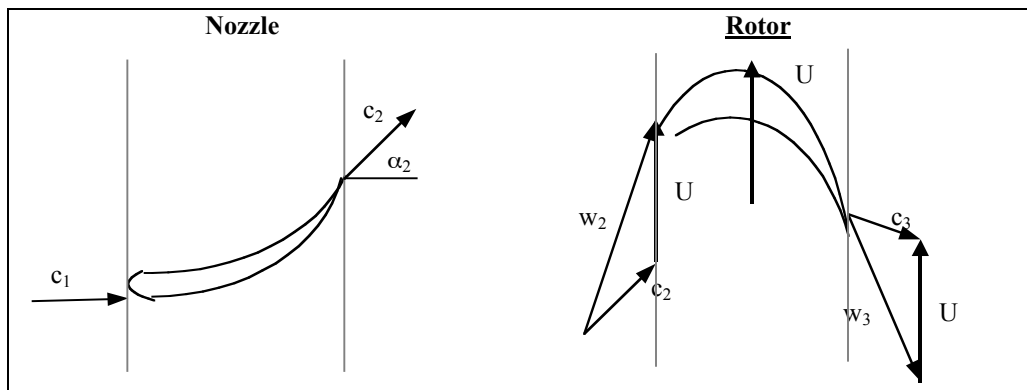


Figure 6A. Turbine stage velocity diagrams

³ Dixon, S.L., *Fluid Mechanics and Thermodynamics of Turbomachinery*, 1998.

Losses

Losses for both the nozzle and the rotor are calculated using correlations and experimental results from the literature¹. The correlations used to calculate the loss coefficient for the nozzle are given in Table 8A, the correlations used to calculate the loss coefficient for the rotor are given in Table 9A. The parameters used in these correlations are the following:

$$\frac{s}{l} = \frac{2\pi r_{pitch}}{L \times n_{b, stator}} \quad \text{and,} \quad \frac{l}{H} = 1.46$$

where, l is the length of the blade, H is the chord, and s is the distance between each blade.

Table 8A. Estimation of impeller losses

Stator		
$\Delta P_{o \text{ loss}} = Y_{s, \text{ total}} (P_{o2s} - P_2)$		
Losses	Equation	Loss Coefficient
Profile loss Coefficient	Fig. 3.25, ⁴	$Y_p = 0.05$
Lift Coefficient ($C_D=0.02$)	$C_L = 2 \frac{s}{l} \cos \alpha_m (\tan \alpha_1 - \tan \alpha_2) - C_D \tan \alpha_m$	2.30
Zweifel Parameter	$Z = \left(\frac{C_L}{s/l} \right)^2 \frac{\cos^2 \alpha_2}{\cos^2 \alpha_m}$	9.36
Secondary Losses	$Y_s = 0.0334 \left(\frac{l}{H} \right) \left(\frac{\cos \alpha_2}{\cos \alpha_1} \right)$	$Y_s = 0.096$
Total Loss Coefficient		$Y_{s, \text{ total}} = 0.146$

Table 9A. Estimation of impeller losses

Rotor		
$\Delta P_{o \text{ loss}} = Y_{s, \text{ total}} (P_{o2s} - P_2)$		
Losses	Equation	Loss Coefficient
Profile loss Coefficient	Fig. 3.25, ¹	$Y_{pr} = 0.11$
Lift Coefficient ($C_D=0.02$)	$C_L = 2 \frac{s}{l} \cos \beta_m (\tan \beta_1 - \tan \beta_2) - C_D \tan \beta_m$	4.10
Zweifel Parameter	$Z = \left(\frac{C_L}{s/l} \right)^2 \frac{\cos^2 \beta_2}{\cos^2 \beta_m}$	11.46
Secondary Losses	$Y_s = 0.0334 \left(\frac{l}{H} \right) \left(\frac{\cos \beta_2}{\cos \beta_1} \right)$	$Y_{sr} = 0.45$
Tip leakage loss	$Y_k = 0.5 \left(\frac{l}{H} \right) \left(\frac{k}{l} \right)^{0.78}$, k is the tip clearance gap = 2.44 mm	$Y_t = 1.78$
Total Loss Coefficient		$Y_{s, \text{ total}} = 2.34$

⁴ Dixon, S.L., *Fluid Mechanics and Thermodynamics of Turbomachinery*, 1998.

Results

The results obtained are in agreement with the results obtained from the radial flow compressor analysis. Certain limitations had to be imposed such as a deviation angle of only 3 deg, and an incidence angle of 5.5 deg. The work output seems in well concordance with the power required by the compressor of the SR-30 engine. The maximum Mach number, at the exit of the nozzle, is quite high, $M_2=0.98$, and some losses not taken into account here, such as shock losses, could be derived from it. The results of the analysis are summarized in Table 10A.

Table 10A. Summary of results

Mass flow rate	$m_{\dot{}}$	0.3 kg/s	Turbine Total to Total Efficiency	$\eta_{tt} = (T01-T03)/(T01-T03_{ss})$	79 %
Reaction	R	0.01	Turbine Adiabatic Efficiency	$\eta_{ts} = (T01-T03)/(T01-T3_{ss})$	75 %
Stator pressure ratio	$p2/p1$	1.92	Stage stagnation pressure ratio	$p03/p01$	2.09
Rotor pressure ratio	$p3/p2$	1.11	Work	$W_{\dot{}}*m_{\dot{}}$	43.5 kW
Incidence Deviation	i –	5.5 deg 3 deg	Exit Stagnation pressure	p03	120 kPa

References

- Cumpsty, N., Compressor Aerodynamics. Longman Scientific and Technical. 1989.
- Dixon, S.L., Fluid Mechanics and Thermodynamics of Turbomachinery, Butterworth-Heinemann, 1998, 4th edition
- Jacobson, S.A., Aerothermal Challenges in the Design of a Microfabricated Turbine Engine, MIT, AIAA-98-2545
- Hill, P., Peterson, C., Mechanics and Thermodynamics of Propulsion. Addison Wesley. 1992.2nd edition.